Available online at www.sciencedirect.com
ScienceDirect
Acta Materialia xxx (2011) xxx–xxx
Acta MATERIALIA
www.elsevier.com/locate/actamat

First-principles study of the nucleation and stability of ordered precipitates in ternary Al–Sc–Li alloys

Z. Mao *, W. Chen, D.N. Seidman, C. Wolverton *

Department of Materials Science and Engineering, Northwestern University, 2220 Campus Drive, Evanston, IL 60208-3108, USA

Received 25 October 2010; received in revised form 14 January 2011; accepted 23 January 2011

Abstract

First-principles density functional calculations are used to study the nucleation and stability of $L1_2$-ordered precipitates in Al–Sc–Li alloys. For dilute Al alloys, there are three possible ordered $L1_2$ precipitates: Al_3Sc, Al_3Li and an Al_3Sc/Al_3Li core/shell structure. To calculate the nucleation behavior, information about bulk thermodynamics (both static total energies and vibrational free energies), interfacial energetics and coherency strain is required. The study finds the following: (1) the coherency strain energies for forming coherent interfaces between Al/Al_3Sc, Al/Al_3Li and Al_3Sc/Al_3Li are relatively small, owing to the small atomic size mismatches in these systems; (2) the sublattice site preferences of Sc and Li are calculated, and it is demonstrated that Sc and Li share the same sublattice sites in both $Al_3Sc(L1_2)$ and $Al_3Li(L1_2)$, in agreement with recent experimental results; (3) the calculated solubilities of Sc and Li in α-Al alloys are in good agreement with experimental values and, for Sc, agree well with prior first-principles results; (4) the interfacial energies for Al/Al_3Sc, Al/Al_3Li and Al_3Sc/Al_3Li for (1 0 0), (1 1 0) and (1 1 1) interfaces are calculated: the values of the Al/Al_3Sc interfacial energies are significantly larger than those of the Al/Al_3Li and Al_3Sc/Al_3Li interfaces; (5) combining the bulk and interfacial energies yields the nucleation barriers and critical radii for Al_3Sc and Al_3Li precipitates; and (6) the energetic stability of the Al_3Sc/Al_3Li core/shell structure is compared with individual Al_3Sc and Al_3Li nuclei, and the range of precipitate sizes for which the core/shell structure is energetically favored is determined quantitatively.

Keywords: Al–Sc–Li; First principles; Interfacial energy; Core/shell structures; Site substitution

1. Introduction

Al-rich Al–Sc–Li alloys are model metallic systems which have many potential applications owing to the significant increase in strength and stiffness compared with pure Al [1–4]. Of all the dilute additions to Al, Sc yields the largest increase in strength on a per atom basis, owing to the formation of a high number density of coherent $Al_3Sc(L1_2)$ precipitates during aging treatments between 300 and 350 °C [5]. Since the solubility of Sc in Al is small, and the cost of Sc is high, there is increasing interest in substituting other elements, such as Li, Cr, Ti, Zr and rare-earth elements for Sc [6].

Each weight per cent of Li added to an Al alloy results in a nearly 3% decrease in density and a 6% increase in Young's modulus, leading to improvements in specific stiffness and a weight savings for structural applications [1]. In addition, there is a large strength increment produced by the formation of metastable and coherent δ'-$Al_3Li(L1_2)$ precipitates, with an achievable volume fraction of up to 30%, owing to the high solubility of Li in Al [7]. Therefore, ternary Al–Sc–Li alloys have the potential for being technologically important alloys with high specific stiffness, improved thermal stability and creep resistance due to Al_3Sc precipitates.

Atom-probe tomography (APT) and transmission electron microscopy studies performed on Al–Sc–Li alloys

* Corresponding authors.
E-mail addresses: z-mao2@northwestern.edu (Z. Mao), wolverton@northwestern.edu (C. Wolverton).

1359-6454/$36.00 © 2011 Acta Materialia Inc. Published by Elsevier Ltd. All rights reserved.
doi:10.1016/j.actamat.2011.01.041

reveal the development of both single-phase α′-$Al_3Sc(L1_2)$ precipitates and metastable δ′-$Al_3Li(L1_2)$ precipitates and complex precipitates consisting of an Al_3Sc core surrounded by a δ′-$Al_3Li(L1_2)$ shell [8–10]. A detailed APT study demonstrates that a two-stage aging treatment initially promotes the nucleation of α′-$Al_3Sc(L1_2)$ at 350 °C. And then as a result of a second aging treatment at 200 °C, larger α′-$Al_3Sc(L1_2)$/δ′-$Al_3Li(L1_2)$ core/shell precipitates are formed, and isolated smaller δ′-$Al_3Li(L1_2)$ precipitates are nucleated. In addition, Li and Sc are found to be partially soluble in the α′-$Al_3Sc(L1_2)$ and δ′-$Al_3Li(L1_2)$ phases, respectively [10,11].

First-principles density functional theory (DFT) calculations were used to study precipitation in these Al–Sc–Li alloys. There are prior theoretical calculations concerning short-range and long-range order, phase equilibra and stabilities of many Al binary systems [12–16]. Binary alloys that form the basis of the Al–Sc–Li system have also been studied by DFT calculations. These previous DFT calculations focused on Al–Sc and Al–Li binary alloys [17–22], and demonstrated that Al/$Al_3Sc(L1_2)$ has significantly larger interfacial energies than does Al/δ′-$Al_3Li(L1_2)$. Additionally, Ozolins et al. calculated accurately the solubility of Sc in Al, and showed that the solubility is strongly dependent on vibrational entropy [18,19,23].

In the present research, results are presented concerning the nucleation stability of $Al_3Sc(L1_2)$ and $Al_3Li(L1_2)$ in Al-rich Al–Sc–Li alloys using first-principles calculations. The solubilities of Sc and Li (with respect to formation of Al_3Sc and Al_3Li, respectively) at different temperatures are determined by calculating the free energies of the dilute solid solution and the ordered $L1_2$ phases. The coherency strains and related interfacial energies for Al/$Al_3Sc(L1_2)$, Al/$Al_3Li(L1_2)$ and $Al_3Sc(L1_2)$/δ′-$Al_3Li(L1_2)$ are also calculated. The stabilities of isolated precipitates and core/shell structures are investigated, and the latter are shown to be energetically stable. Finally, the thermodynamic substitutional path and sublattice site preference of Sc and Li are determined, and it is demonstrated that Sc and Li share the same sublattice sites, in agreement with APT results [10].

2. Computational methodology

DFT calculations employed plane-wave total-energy methodology with both local density approximation (LDA) [24] and generalized gradient approximation (GGA) [25] for exchange correlation, as implemented in the Vienna *ab initio* simulation package (VASP) [26–30]. The projector augmented wave (PAW) potentials was used [31]. Unless otherwise specified, all structures were fully relaxed with respect to volume as well as all cell–internal atomic coordinates. The convergence of results with respect to energy cutoff and *k*-points was carefully considered. A plane-wave basis set was used with an energy cutoff of 300 eV to represent the Kohn–Sham wave functions. The summation over the Brillouin zone for the bulk structures is performed on a 0.13 (1/Å) spacing Monkhorst–Pack *k*-point mesh for all calculations.

The vibrational thermodynamic properties are essential for calculating the temperature dependence of the solubilities and nucleation energies of Sc and Li in Al. The harmonic approximation was used for all vibrational calculations. To calculate the phonon dispersions for the solubility of Sc and Li in Al, the frozen-phonon method was used [32–34] to compute the vibrational thermodynamics for dilute solutions of Sc or Li in Al, as well as for the Al_3Li andAl_3Sc phases. For the Sc or Li dilute solid solution Al_nZ ($n = 31$, Z = Sc or Li), a 32-atom cubic cell ($2 \times 2 \times 2$ conventional cubes of face-centered cubic (fcc)) was used with either a Sc or Li atom replacing Al on the central site. For the Al_3Sc and Al_3Li phases, supercells of $3 \times 3 \times 3$ cubic units cells, comprising 108 total atoms, were used. The vibrational free energies of these cells are obtained from the phonon density of states using standard thermodynamic expressions.

3. Results and discussion

This paper presents calculations of the nucleation barriers and stability of core/shell structures in Al–Sc–Li alloys. To accomplish this, the energetic and thermodynamic properties of the bulk phases, as well as the interfacial energies, needed to be determined. First, the first-principles results of the bulk properties are discussed, including the formation energies of the $L1_2$ structures, lattice parameters, elastic constants and strain energies, and subsequently the calculated interfacial energies are discussed. From these results, a more complete physical picture of the energetics of nucleation of $L1_2$ structures in dilute Al–Sc–Li alloys is obtained. These energies permit an understanding of the stability of both isolated and core/shell precipitates, and for the prediction of the stable precipitate morphology in dilute Al–Sc–Li alloys.

3.1. Bulk properties: the ground states of ordered Al_3Sc and Al_3Li

This section commences with results for the ground-state stability of Al_3Sc and Al_3Li in different commonly occurring intermetallic crystal structures. Four-types of ordered structures for Al_3Sc and Al_3Li are considered: $L1_2$, DO_{19}, DO_{22} and DO_{23}. There are prior first-principles calculations for $Al_3Sc(L1_2)$ and δ′-$Al_3Li(L1_2)$ (e.g., Ref. [35]), and the present methodology is compared with previous calculations and experiments to determine the degree of agreement. The calculated formation energies are listed in Table 1. The agreement between first-principles and experimental formation energies [19,35–37] for the stable ordered structures for Al_3Sc is good, and there is only a small (~10%) but systematic deviation between the LDA and GGA results. Both LDA and GGA demonstrate correctly that the experimentally observed $L1_2$ structure is the lowest-energy structure for both Al_3Sc and metastable

Please cite this article in press as: Mao Z et al. First-principles study of the nucleation and stability of ordered precipitates in ternary Al–Sc–Li alloys. Acta Mater (2011), doi:10.1016/j.actamat.2011.01.041

Table 1
DFT calculated formation energies (eV per solute atom) of Al_3Sc and Al_3Li for the $L1_2$, DO_{23}, DO_{19} and DO_{22} structures, using GGA and LDA methods; calculated values are compared with previous calculations and experimental data, when available.

	Al_3Sc			Al_3Li		
	Literature values	LDA	GGA	Literature values	LDA	GGA
$L1_2$	−1.96[a], 1.99[b], 1.80[c]	−1.99	−1.81	−0.41[d], −0.43[e]	−0.44	−0.39
DO_{23}	–	−1.79	−1.63	–	−0.41	−0.36
DO_{19}	–	−1.73	−1.57	–	−0.33	−0.28
DO_{22}	−1.53[b]	−1.57	−1.44	–	−0.39	−0.34

[a] LDA VASP, Ref. [35].
[b] LDA VASP, Ref. [19].
[c] Experimental data [38,39].
[d] LDA VASP, Ref. [35].
[e] COST507 CALPHAD database [35].

δ′-Al_3Li. DO_{23} is the second lowest-energy structure among the four for Al_3Sc and Al_3Li. DO_{22} and DO_{19} are the least-stable structures for Al_3Sc and Al_3Li, respectively. The calculated lattice parameters are: 4.032 Å (GGA) and 3.982 Å (LDA) for fcc Al; 4.103 Å (GGA) and 4.027 Å (LDA) for $Al_3Sc(L1_2)$; and 4.021 Å (GGA) and 3.965 Å (LDA) for δ′-$Al_3Li(L1_2)$, which are in good agreement with the experimental results (Table 2). The calculated lattice parameter mismatch is 1.7% for Al/$Al_3Sc(L1_2)$, 0.2% for Al/$Al_3Li(L1_2)$ and 2.0% for $Al_3Sc(L1_2)$/$Al_3Li(L1_2)$ employing GGA calculations. These lattice parameter mismatches are small, and the relative values for the three systems are qualitatively consistent with (but smaller than) experimental values: 2.2% for Al(fcc)/$Al_3Sc(L1_2)$; 0.9% for Al(fcc)/$Al_3Er(L1_2)$; and 0.75% for Al(fcc)/$Al_3Zr(L1_2)$.

3.2. Bulk properties: elastic constants and coherency strain energies of Al, Al_3Sc and Al_3Li

Calculations of the bulk elastic constants and coherency elastic strain energies assuming coherent interfaces are described next. The lattice parameter mismatch at a coherent interface results in a coherency elastic strain energy which affects nucleation behavior, among other things. The coherency elastic strain energy is related to the energy of deformation of the phases for specific interfacial orientations. The strain between ordered precipitates and the disordered matrix has important effects on the nucleation behavior, coherent phase stability and other properties. In harmonic elasticity theory, this elastic strain energy is related to the elastic constants. The bulk modulus B can be calculated from first-principles total energy calculations by considering a hydrostatic deformation. The three elastic constants C_{11}, C_{12} and C_{44} of a cubic crystal are determined by either tetragonal or trigonal lattice distortions [40]. The bulk modulus B, the anisotropy ratio A and the Voigt averaged shear modulus $\langle G_v \rangle$ are given by

$$B = \frac{C_{11} + 2C_{12}}{3} \quad (1)$$

$$A = \frac{2C_{44}}{C_{11} - C_{12}} \quad (2)$$

$$\langle G_v \rangle = \frac{3C_{44} + C_{11} - C_{12}}{5} \quad (3)$$

The calculated elastic constants B, A and $\langle G_v \rangle$ of Al, $Al_3Sc(L1_2)$ and $Al_3Li(L1_2)$ are listed in Table 2. The values are in good agreement with experimental results and prior first-principles calculations [19,41]. It is found that Al_3Sc has the largest elastic constants, and Al_3Li has the smallest ones, with Al being intermediate between them.

It is difficult to obtain completely reliable experimental results for the bulk properties, particularly the elastic properties, of metastable δ′-$Al_3Li(L1_2)$. First-principles elastic constants are therefore valuable, although prior calculations yielded inconsistent results. Guo et al. [40] reported a first-principles LDA value of $C_{11} = 158$ GPa, which is larger than the experimental value, 123.6 GPa. Alternatively, Li et al. [42] calculated LDA values of C_{12} and C_{44} of 57.1 and 70.4 GPa, respectively, which are significantly larger than the experimental values of 37.2 and 42.8 GPa. Calculated GGA results for δ′-$Al_3Li(L1_2)$ are

Table 2
Lattice parameter a_o, bulk modulus B, elastic constants C_{ij}, anisotropy ratio A and Voigt averaged shear modulus $\langle G_v \rangle$ from first-principles calculations (GGA); the results are compared with previous DFT calculations and experimental values (Exp.).

	Al			Al_3Sc			Al_3Li		
	Exp.	GGA	DFT	Exp.	GGA	DFT	Exp.	GGA	DFT
a_0 (Å)	4.010[a]	4.032	3.973[a]	4.101[b]	4.103	4.038[b]	3.972[c]	4.021	3.949[c]
C_{11} (GPa)	124[a]	109	106.1[a]	183[b]	188	191[b]	123.6[c]	122	158.0[d], 123.6[c]
C_{12} (GPa)	61.9[a]	64.5	68.6[a]	46.0[b]	43.7	43.0[b]	37.2[c]	33.3	29.4[d], 37.2[c]
C_{44} (GPa)	31.6[a]	32.4	33.6[a]	68[b]	71.4	82.0[b]	42.8[c]	52.3	57.7[d], 66.0[c]
B (GPa)	79.3[a]	79.3	79.2[a]	91.7[b]	91.8	91.6[b]	66.0[c]	62.9	72.3[d]
A	1.21[a]	1.46	1.529[a]	0.99[b]	0.99	0.99[b]	1.01[c]	1.18	0.897[d]
$\langle G \rangle_V$ (GPa)	29.4[a]	28.3	–	68.2[b]	71.7	–	43.0[c]	49.2	60.3[d]

[a] Experimental data and LDA DFT calculations from Ref. [42].
[b] Experimental data and LDA DFT calculations from Ref. [41].
[c] Experimental data and LDA DFT calculations from Ref. [42].
[d] LDA DFT calculations from Ref. [40].

Please cite this article in press as: Mao Z et al. First-principles study of the nucleation and stability of ordered precipitates in ternary Al–Sc–Li alloys. Acta Mater (2011), doi:10.1016/j.actamat.2011.01.041

displayed in Table 2 and are significantly closer to the experimental results than previous calculations. The authors suspect that the differences are because GGA yields better values than LDA does for these systems.

This study now turns to the coherency elastic strain energies, and they are calculated for Al/$Al_3Sc(L1_2)$, Al/$Al_3Li(L1_2)$ and $Al_3Sc(L1_2)$/$Al_3Li(L1_2)$ for different strain orientations. One can visualize this coherency strain as the formation energy of coherent long-period A_pB_q superlattices, which are non-zero and depend on the superlattice direction $\hat{G}$. In the long-period limit p, $q \to \infty$, and the interfacial energy becomes negligibly small in comparison with the elastic strain energy needed to deform the constituents to a common in-plane lattice constant a_S. The constituent strain energy is precisely this long-period superlattice energy, and has been calculated previously using DFT calculations for a number of systems [14,15,43–51]. The following procedure is followed as used in these previous studies.

The formation energy per atom of an $A_\infty B_\infty$ superlattice along $\hat{G}$ with composition x is given by the constituent strain energy $\Delta E^{eq}_{CS}(x, \hat{G})$, defined as the equilibrium value of the composition-weighted sum of the energies required to deform bulk A and B to the epitaxial geometry with a planar lattice constant a_S perpendicular to $\hat{G}$ as given by [44]

$$\Delta E^{eq}_{CS}(x, \hat{G}) = \min_{a_S}[x\Delta E^{epi}_A(a_S, \hat{G}) + (1-x)\Delta E^{epi}_B(a_S, \hat{G}) \quad (4)$$

where a_S is the constrained superlattice parameter, $\hat{G}$ is the direction, x is the mole fraction of phase A, ΔE^{epi}_A and Δ^{epi}_B are the epitaxial deformation energies of phases A and B, respectively. The energy $E^{epi}_A(a_S, \hat{G})$ corresponds to the energy required to deform epitaxially material A to the lattice constant a_S in the plane orthogonal to $\hat{G}$, and permits it to relax along $\hat{G}$. The epitaxial deformation energy is related to the epitaxial softening function:

$$q(a_S, \hat{G}) = \frac{\Delta E^{epi}(a_S, \hat{G})}{\Delta E^{bulk}(a_S)} \quad (5)$$

$\Delta E^{bulk}(a_S)$ is the energy required to deform hydrostatically a bulk solid to the lattice constant a_S. DFT calculations yield the anharmonic strain energies from $\Delta E^{epi}_A(a_S, G)$.

The coherency strain energies were calculated for Al/$Al_3Sc(L1_2)$, Al/$Al_3Li(L1_2)$ and $Al_3Sc(L1_2)$/$Al_3Li(L1_2)$ for the [1 0 0], [1 1 0] and [1 1 1] directions (Fig. 1). For the systems involving $Al_3Sc(L1_2)$, it is found that the [1 0 0] direction is the elastically softest direction (that is, the one with the smallest coherency strain energy). Al/$Al_3Sc(L1_2)$ has the largest elastic strain energy among the three systems. The strain energies of $Al_3Sc(L1_2)$/$Al_3Li(L1_2)$ are about half the magnitude of Al/$Al_3Sc(L1_2)$. Al/$Al_3Li(L1_2)$ has extremely small strain energies and, surprisingly, the [1 1 1] direction exhibits the smallest strain energy. Since the strain energy in this system is extremely small, the numerical noise in the calculations may be responsible for this unusual elastically soft direction.

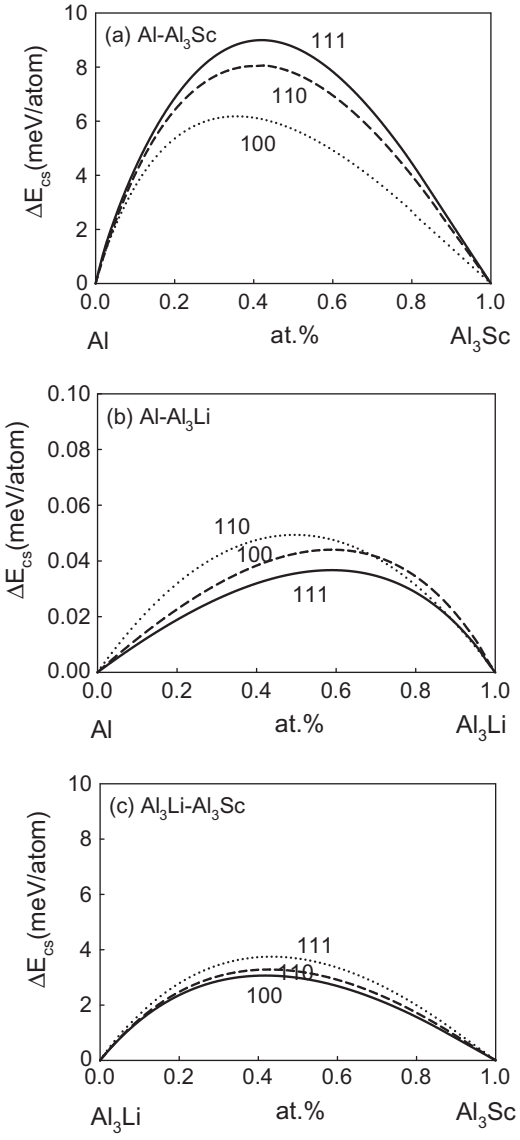

Fig. 1. Calculated equilibrium coherency strain energies for: (a) Al/$Al_3Sc(L1_2)$ (lattice parameter misfit: 1.7% from GGA and 2.2% from experiments); (b) Al/$Al_3Li(L1_2)$ (lattice parameter misfit: 0.2% from GGA and 0.9% from experiments); and (c) $Al_3Sc(L1_2)$/$Al_3Li(L1_2)$ (lattice parameter misfit: 2.0% from GGA and 3.0% from experiments). All the strain energies are small in comparison with the chemical driving force ΔF_{chem} for $Al_3Sc(L1_2)$ and $Al_3Li(L1_2)$. The calculations were performed for the (1 0 0), (1 1 0) and (1 1 1) planes.

3.3. Bulk properties: sublattice site preference and substitution pathways of Sc and Li

There are two experimentally observed precipitate phases in dilute Al–Sc–Li alloys, $Al_3Sc(L1_2)$ and δ′-$Al_3Li(L1_2)$, which is consistent with the ground state calculations: specifically, the $L1_2$ structure has the smallest formation energies for $Al_3Sc(L1_2)$ and δ′-$Al_3Li(L1_2)$ [52]. The $Al_3Z(L1_2)$ (Z = Sc or Li) structure has two different sublattice sites, Al and Z. It has been determined experimentally that, in the ternary system, neither $Al_3Sc(L1_2)$ nor δ′-$Al_3Li(L1_2)$ are perfectly stoichiometric. The precipi-

Please cite this article in press as: Mao Z et al. First-principles study of the nucleation and stability of ordered precipitates in ternary Al–Sc–Li alloys. Acta Mater (2011), doi:10.1016/j.actamat.2011.01.041

tates contain both Li and Sc, respectively, as determined by APT [10]. It is therefore important to understand the sublattice site preferences of Sc and Li, and the substitutional pathways involved in $L1_2$ precipitation. Site substitution energies are computed using $2 \times 2 \times 2$ (32 atoms) Al_3Sc (or Al_3Li) fully relaxed supercells. The substitutional structures were modeled by allowing Li (or Sc) to substitute on two different sublattice sites, either Al or Z (Sc or Li), in the $Al_3Sc(L1_2)$ (or $Al_3Li(L1_2)$) superlattice, and allowing the structures to relax fully. The substitutional energies, $E^{Al_3Sc}_{Li\to Al}$ and $E^{Al_3Sc}_{Li\to Sc}$ in Al_3Sc, and $E^{Al_3Li}_{Sc\to Al}$ and $E^{Al_3Li}_{Sc\to Li}$ in Al_3Li, are defined as follows:

$$E^{Al_3Sc}_{Li\to Al} = \left[\left(E^{tot}_{(Al_{1-x}Li_x)_3Sc} + n_{Al}\mu_{Al}\right) - \left(E^{tot}_{Al_3Sc} + n_{Li}\mu_{Li}\right)\right]\Big/ n_{Li} \quad (6)$$

$$E^{Al_3Sc}_{Li\to Sc} = \left[\left(E^{tot}_{Al_3(Sc_{1-y}Li_y)} + n_{Sc}\mu_{Sc}\right) - \left(E^{tot}_{Al_3Sc} + n_{Li}\mu_{Li}\right)\right]\Big/ n_{Li} \quad (7)$$

$$E^{Al_3Li}_{Sc\to Al} = \left[\left(E^{tot}_{(Al_{1-x}Sc_x)_3Li} + n_{Al}\mu_{Al}\right) - \left(E^{tot}_{Al_3Li} + n_{Sc}\mu_{Sc}\right)\right]\Big/ n_{Sc} \quad (8)$$

$$E^{Al_3Li}_{Sc\to Li} = \left[\left(E^{tot}_{Al_3(Li_{1-y}Sc_y)} + n_{Li}\mu_{Li}\right) - \left(E^{tot}_{Al_3Li} + n_{Sc}\mu_{Sc}\right)\right]\Big/ n_{Sc} \quad (9)$$

where E^{tot} is the calculated total energy before and after substitution, n is the number of substitutional atoms, x and y are the fractions substituted (this research uses only one substitutional atom, so $x = 1/24$ and $y = 1/8$), and μ is the chemical potential. The chemical potentials need to be chosen carefully because of the different substitutional paths. Two possible reference states were considered: (1) a dilute solid solution Al_nZ ($n = 31$); and (2) the equilibrium $Al_3Z(L1_2)$ phase. For a dilute solution, the chemical potential is calculated from the dilute solution $Al_{31}Z$ and pure Al: $\mu_Z = E_{Al_{31}Z} - 31E_{Al}$. For equilibrium Al_3Z, the chemical potential is calculated from Al_3Z and pure Al: $\mu_Z = E_{Al_3Z} - 3E_{Al}$. The chemical potential values of Li and Sc are -2.26, -7.43 eV atom^{-1} for a dilute solution and -2.30, -8.15 eV atom^{-1} for the equilibrium $Al_3Z(L1_2)$ phase.

The choice of the chemical potential used is determined for each specific substitutional path, for which there are four possible pathways for each solute element. The pathways for the substitution of Li in $Al_3Sc(L1_2)$, for example, are as follows: (1) Li from the solid solution occupies the Al or Sc sublattice site in $Al_3Sc(L1_2)$, and the substituted atom (Al or Sc) goes into the solid solution; (2) Li from the solid solution substitutes for Al or Sc in $Al_3Sc(L1_2)$, and the atom substituted for forms additional $Al_3Sc(L1_2)$; (3) Li from $Al_3Li(L1_2)$ substitutes for Al or Sc in $Al_3Sc(L1_2)$, and the atom substituted for goes into solid solution; and (4) Li from $Al_3Li(L1_2)$ substitutes for Al or Sc, which subsequently forms additional Al_3Sc. Similar calculations were performed for Sc substitution in $Al_3Li(L1_2)$. The calculated substitutional energies are listed in Table 4. It is energetically favorable for Li to occupy Sc sublattice sites in $Al_3Sc(L1_2)$, and for Sc to occupy the Li sublattice site in $Al_3Li(L1_2)$, which is in agreement with APT experiments showing that Li and Sc share the same sublattice sites [10]. The second substitutional pathway, whereby the substitution of a solute element from the solid solution results in the formation of additional $Al_3Z(L1_2)$, has the smallest substitutional energy for both Li substitution in $Al_3Sc(L1_2)$ and Sc substitution in $Al_3Li(L1_2)$: -0.059 eV and -0.028 eV atom^{-1}, respectively.

3.4. Bulk properties: the solubility of Sc and Li in Al solid solution

The phase fraction of precipitates that can form in a solid solution is dependent on the solute concentration and the solute solubility at given temperature. The calculation of solute solubility from first principles is a very sensitive test of the accuracy of the present methods. Ozolins and Asta [23] demonstrated previously that a quantitatively accurate prediction of the solvus curve is possible for the Al–Sc system. They also demonstrated that the effect of vibrational thermodynamics on the solvus curve is large, and it increases the solubility by more than an order of magnitude. Subsequently, solvus curves for other Al alloys have been computed from first principles, including Al–Cu [13] and Al–Si [17], and the role of vibrational entropy in these systems was also found to be large. Therefore, the vibrational contributions are crucial for a first-principles calculation of solubility. The first-principles Al–Sc solvus curve calculations were repeated, and the calculations to the Al–Li system extended.

The solubility limits of Sc or Li in Al(fcc) is calculated using the ideal solution equation with the Al_3Z (Z = Sc or Li) phase treated as a stoichiometric line compound and the solid-solution phase is taken as dilute. The solvus curve between bulk Al and the Al_3Z phases is then given by

$$c_s = \exp\left[\frac{\Delta G(Al_3Z) - \Delta G(Al_nZ)}{k_BT}\right] = \exp\left[\frac{\Delta H(Al_3Z) - \Delta H(Al_nZ)}{k_BT}\right]\exp\left[\frac{\Delta S(Al_3Z) - \Delta S(Al_nZ)}{k_B}\right] \quad (10)$$

where k_B is Boltzmann's constant, $\Delta G(Al_3Z)$ and $\Delta G(Al_nZ)$ are the Gibbs free energies of formation per solute atom Z for the Al_3Z supercell and for a single Z impurity atom in Al(fcc), respectively. ΔH and ΔS are the corresponding enthalpy and entropy contributions to the Gibbs free energy of formation $\Delta G(Al_3Z)$ and $\Delta G(Al_nZ)$. A negative enthalpy contribution means that ordered Al_3Z dissolves into Al_nZ ($n = 31$). The first-principles excess enthalpy (Table 3), $\Delta H(Al_3Z) - \Delta G(Al_nZ)$, is -0.72 eV solute atom^{-1} for Al_3Sc at 0 K, which is in excellent agreement with the values -0.72 [52], -0.76 [19] and -0.77 [35] eV solute atom^{-1} determined from experimental solvus curves by Hatch [52], calculations by Asta and

Table 3
DFT results for the excess enthalpies, equilibrium volumes per atom, and vibrational excess entropies related to $L1_2$-ordered Al_3Sc and Al_3Li, dilute solid solutions Al_nSc and Al_nLi.

	ΔH_0 (eV solute atom^{-1})	V_0 (Å^3)	ΔS_{vib} (k_B solute atom^{-1})	
			DFT (this work)	Ozolins et al. [17]
Al_3Sc	−1.815	17.27	−2.48	−2.80
$Al_{31}Sc$	−1.094	16.87	0.18	0.15
Al_3Li	−0.394	16.35	−0.38	–
$Al_{31}Li$	−0.275	16.40	0.09	–
fcc Al	0.00	16.44	0.00	0.00

Table 4
DFT calculated substitutional formation energies (eV per substitutional atom) of Li and Sc in $L1_2$-ordered Al_3Sc and Al_3Li, respectively. A substitutional atom (for example, Li) either from solid-solution Al_nLi or from $Al_3Li(L1_2)$. After substitution, the substituted atom, either goes into solid solution or forms additional $Al_3Z(L1_2)$. From the calculations, the substitutional path is that a Li atom from solid solution prefers substituting for a Sc atom, and the substituted Sc atom forms additional Al_3Sc. Scandium has the same substitutional pattern.

Substituting element	Substituted element	Solution (eV atom^{-1})	Al_3Z (eV atom^{-1})
Li (Al_nLi)	Al(in Al_3Sc)	0.556	0.556
	Sc(in Al_3Sc)	0.459	−0.059 (preferred)
Li (Al_3Li)	Al(in Al_3Sc)	0.593	0.593
	Sc(in Al_3Sc)	0.696	−0.022
Sc (Al_nSc)	Al(in Al_3Li)	1.124	1.124
	Sc(in Al_3Li)	0.878	−0.028 (preferred)
Sc (Al_3Sc)	Al(in Al_3Li)	1.265	1.265
	Sc(in Al_3Li)	0.925	0.019

Ozolins [19] and Wolverton and Ozolins [35], respectively. For $Al_3Li(L1_2)$, the calculated excess enthalpy of -0.12 eV atom^{-1} lies between the -0.28 eV atom^{-1} [52] and -0.04 eV atom^{-1} values [35], respectively.

The vibrational entropy $\Delta S(Al_3Z) - \Delta S(Al_nZ)$ contribution to solubility is discussed next. The harmonic phonon dispersions of Al(fcc), Sc(hcp), Li(bcc), dilute fcc solid solutions (Al_nSc and Al_nLi), and $Al_3Sc(L1_2)$ and $Al_3Li(L1_2)$ were determined. The formation enthalpies and vibrational entropies are listed in Table 3. A $3 \times 3 \times 3$ superlattice was used for the vibrational entropy calculations for both Sc(hcp) (total 27 atoms) and Li(bcc) (total 27 atoms). The compounds $Al_3Sc(L1_2)$ and $Al_3Li(L1_2)$ have negative vibrational formation entropies, while Al_nSc and Al_nLi have positive vibrational entropies. These results are in excellent agreement with prior calculations for Sc [17,53,54]. To the authors' knowledge, analogous calculations have not been performed for Al–Li alloys. The difference in excess entropies is $2.66k_B$ and $0.47k_B$ for Sc and Li, respectively, which corresponds to $\Delta S_{vib} = 22.12$ J K^{-1} mol^{-1} and 3.87 J K^{-1} mol^{-1}. These values yield an approximate 14-fold increase in the calculated solubility of Sc in Al and an approximate twofold increase in the calculated solubility of Li in Al compared with the static calculations without vibrations. The solubilities with and without vibrational entropies are presented in Figs. 2 and 3 for Al–Sc and Al–Li, respectively, where they are compared with experimental results. In agreement with the work of Asta and Ozolins [23], it is confirmed that the calculated solubility of Sc is in excellent agreement with experiment [52,55–57], if the effects of vibrational entropies are included.

The vibrational entropies play a smaller role in the Li solubility calculations. In the Al–Li system, the experimentally measured solvus curves of the metastable δ′-$Al_3Li(L1_2)$ phase exhibit significant scatter. Specifically, the experimentally measured solubility [58–75] ranges from 2 to 14 at.% Li from 100 to 350 °C, with a significant uncertainty for each measured solubility, owing to the metastability of the δ′-$Al_3Li(L1_2)$ phase. Despite this uncertainty, the first-principles calculated solvus curve of Li in Al is in good agreement with the measured values. This agreement is somewhat surprising, since the present calculations employ a dilute-solution approximation, whereas the solu-

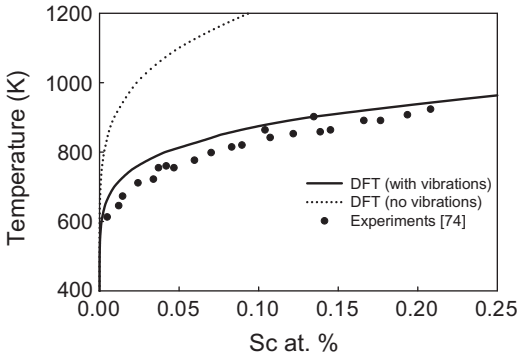

Fig. 2. The experimental and first-principles solvus curves for Al-rich Al–Sc alloys. The solvus curves were calculated both with and without a contribution from vibrational thermodynamics. The contribution from vibrational entropy is significant, and the inclusion of vibrational effects brings the DFT calculated solvus curve into excellent agreement with experiments [83] and prior calculations [23].

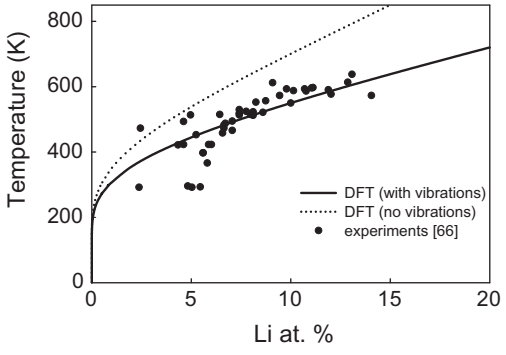

Fig. 3. The experimental and first-principles solvus curves for Al-rich Al–Li alloys. The solvus curves were calculated both with and without the contribution due to vibrational thermodynamics. The contribution from vibrational entropy is significant and the inclusion of vibrational effects brings the DFT calculated solvus curve into good agreement with experiments [75].

Please cite this article in press as: Mao Z et al. First-principles study of the nucleation and stability of ordered precipitates in ternary Al–Sc–Li alloys. Acta Mater (2011), doi:10.1016/j.actamat.2011.01.041

bility of Li in Al is relatively large. The solvus curve calculations for Al–Sc and Al–Li give the present authors confidence in the quantitative accuracy of their first-principles thermodynamic calculations.

3.5. Interfacial properties: energies of Al/Al_3Sc, Al/Al_3Li and Al_3Sc/Al_3Li interfaces

The interfacial energies between different phases are critical for determining the mechanisms that lead to the nucleation of precipitates with the $L1_2$ structure from a disordered fcc solid solution. In contrast to the case of a binary alloy, the precipitation in dilute Al–Sc–Li alloys is complicated by the different observed precipitate morphologies. For instance, experimentally, during a two-stage aging treatment, both α′-$Al_3Sc(L1_2)$ and δ′-$Al_3Li(L1_2)$ precipitates are observed in the first stage at 350 °C, and a core/shell structure precipitate, $Al_3Sc(L1_2)/Al_3Li(L1_2)$, is observed in the second aging stage at 200 °C [10]. The first aging stage yields the following precipitate/matrix interfaces: $Al/Al_3Sc(L1_2)$ and $Al/Al_3Li(L1_2)$. In the core/shell precipitates, an additional interface is formed between the core and the shell, that is, $Al_3Sc(L1_2)/Al_3Li(L1_2)$. These core/shell interfacial energies are currently unknown.

Interfacial energies were calculated employing the first-principles supercell approach. Since the values of the lattice parameter mismatches of the phases present in Al–Sc–Li are small (<2%), the interfacial structures are treated as coherent. Three interfaces were constructed: $Al/Al_3Sc(L1_2)$, $Al/Al_3Li(L1_2)$ and $Al_3Sc(L1_2)/Al_3Li(L1_2)$. And for each interface the energies were determined for the (1 0 0), (1 1 0) and (1 1 1) interfacial orientations. The interfacial configurations were constructed with the initial positions on an ideal and uniform fcc lattice with a lattice parameter of 4.037 Å for both phases. Subsequently, all atomic positions, cell vectors and volume were fully relaxed, and it was found that the relaxation can be accomplished more efficiently using a two-step procedure: (1) initially relax all atoms and the cell vector in the direction perpendicular to the interface; and subsequently (2) relax all degrees of freedom fully both perpendicular and parallel to the interface plane. There are two equivalent interfaces in each supercell, and a supercell with a separation of $3a$ lattice parameters between these two interfaces was found to be sufficient to ensure the convergence of the interfacial energy calculations.

The interfacial internal energies are calculated by subtracting the total energy of the phases on either side of the interface from the total energy of a two-phase system containing an interface:

$$\gamma_{\alpha/\beta} = \frac{1}{2S}\left[E^{tot}_{\alpha/\beta} - \left(E^{tot}_{\alpha} + E^{tot}_{\beta}\right) - \Delta E_{cs}\right] \tag{11}$$

where S is the interfacial area, the subscripts α and β denote the two phases across the interface plane (Al, Al_3Sc or Al_3Li); $E^{tot}_{\alpha/\beta}$ is the total internal energy of the relaxed α/β system containing an interface; E^{tot}_{α} and E^{tot}_{β} are the total internal energies of phases α and β, respectively, each relaxed to their own equilibrium geometry; and ΔE_{CS} is the coherency strain energy between α and β (Fig. 1). The technique of calculating interfacial energy including strain effects is described by Wolverton and Zunger [76]. The resulting calculated interfacial energies for both LDA and GGA are listed in Table 5. Prior research for Al–Sc and Al–Li alloys reported interfacial energy calculations using LDA [77,78]. To the authors' knowledge, a systematic comparison of interfacial energies employing LDA and GGA has not been reported. From the calculations, it is found that the calculated interfacial energies using GGA are similar to those calculated employing LDA. There is, however, a small systematic shift of the GGA interfacial energies predicting consistently smaller interfacial energies than does LDA. This systematic shift is consistent with the well-known tendency of LDA to predict overbinding for a wide range of properties (for example, lattice parameters and elastic constants). GGA is often found to correct the overbinding and, specifically, GGA predicts smaller interfacial energies than does LDA, consistent with weaker binding energies of atoms across the interface plane. The $Al/Al_3Sc(L1_2)$ interface has the largest calculated interfacial energy, while the $Al/Al_3Li(L1_2)$ interfacial energy has the smallest value, in agreement with prior LDA calculations [21,79]. The (1 0 0) interface is generally found to have the smallest interfacial energy, because it does not break any Al–transition metal bonds. The (1 0 0) interface has a smaller interfacial energy than do the (1 1 0) and (1 1 1) interfacial planes, in agreement with high resolution electron microscopy results, which demonstrates that $Al_3Sc(L1_2)$ precipitates develop large (1 0 0) facets and small (1 1 0) and (1 1 1) facets as they nucleate, grow and coarsen [3]. Using the Wulff construction and the calculated interfacial energies, it can be shown that the equilib-

Table 5
DFT calculated interfacial energies of three different interfaces (1 0 0), (1 1 0) and (1 1 1), using both LDA and GGA exchange correlations (mJ m^{-2}).

Type	[1 0 0]			[1 1 0]			[1 1 1]		
	Literature	LDA	GGA	Literature	LDA	GGA	Literature	LDA	GGA
Al/Al_3Sc	192[a]	176	165	–	193	178	226[a]	203	189
Al/Al_3Li	16[b]	14	12	22[b]	20	17	27[b]	26	22
Al_3Li/Al_3Sc	–	94	83	–	106	93	–	113	101

[a] LDA DFT Refs. [19,78].
[b] LDA DFT Ref. [77].

Please cite this article in press as: Mao Z et al. First-principles study of the nucleation and stability of ordered precipitates in ternary Al–Sc–Li alloys. Acta Mater (2011), doi:10.1016/j.actamat.2011.01.041

rium morphology of an Al_3Sc precipitate is a great rhombicuboctahdron [3,53]. In Section 3.6, the (1 0 0) interfacial energies are used to calculate the critical net reversible work and critical radius required for nucleation and to model the stability of the core/shell structure [3]. It is emphasized that these interfacial energies were calculated for a sharp interface at 0 K, and that the $T = 0$ K values overestimate the temperature-dependent interfacial free energy. For example, Asta et al. estimated the entropic contribution to the $Al/Al_3Sc(L1_2)$ interfacial energy, and found that the values of interfacial energy decreases most significantly for the (1 1 1) plane as temperature increases and only slightly decreases for (1 0 0) plane at 1000 K [78].

3.6. Nucleation properties: first-principles nucleation barriers and critical radii for $Al_3Sc(L1_2)$ and $Al_3Li(L1_2)$

According to classical nucleation theory (CNT), the thermodynamic barrier to nucleation is controlled by competition among: (1) a negative bulk volume free energy contribution, which is the chemical formation Helmholtz free energy change ΔF_{chem}; (2) a positive elastic internal strain energy $\Delta E_{elastic}$; and (3) a positive interfacial free energy contribution γ [80,81]. Using CNT, the study aimed to understand the thermodynamics for nucleation of $Al_3Sc(L1_2)$ and $Al_3Li(L1_2)$ in an Al matrix. The first-principles calculations for the bulk, strain and interfacial energies of these systems, which are required to calculate the barrier to nucleation, are described above. And now these quantities are assembled into a first-principles prediction of nucleation thermodynamics of $Al_3Sc(L1_2)$ and $Al_3Li(L1_2)$ precipitates.

First, isolated homogeneous nucleation of spherical precipitates is considered. The reversible work for the formation of a spherical nucleus W_R^{homo} as a function of nucleus radius R is given by [53,82]

$$W_R^{homo} = \frac{4\pi}{3} R^3 \Delta F_V + 4\pi R^2 \gamma \tag{12}$$

where

$$\Delta F_V = \Delta F_{chem} + \Delta E_{elastic} \tag{13}$$

The critical radius R^* for nucleation is given by

$$R^* = \frac{-2\gamma}{\Delta F_{chem} + \Delta E_{elastic}} \tag{14}$$

and the critical net reversible work required for the formation of a critical spherical nucleus $W_R^{homo}(R^*)$ with radius R^* is given by

$$W_R^{homo}(R^*) = \frac{16\pi}{3} \frac{\gamma^3}{(\Delta F_{chem} + \Delta E_{elastic})^2} \tag{15}$$

The chemical formation energies were calculated based on the nucleation of Al_3Z $(L1_2)$ from a dilute solid solution, $Al_nZ \rightarrow Al_3Z + Al_{n-3}$, where $Z = Sc$ or Li, and $n = 31$. The equation for ΔF_{chem} is given by

$$\begin{aligned} \Delta F_{chem} &= \Delta F(Al_3Z) + (n-3)\Delta F(Al) - \Delta F(Al_nZ) \\ &= [\Delta H(Al_3Z) - \Delta H(Al_nZ)] - T[\Delta S(Al_3Z) \\ &\quad - \Delta S(Al_nZ)] \end{aligned} \tag{16}$$

The enthalpy H is taken to be equal to the internal energy E, because in the solid state the pressure–volume term in H is negligible compared with E. The entropy terms in Eq. (16) are from the vibrational entropies of the ordered Al_3Z and Al_nZ cells calculated above. In dilute Al_nZ solution, since the configurational entropy is much smaller in comparison with vibrational entropy, its contribution was not considered. Using Eq. (16), the calculated values of ΔF_{chem} at 350 °C are -45.9 meV atom^{-1} (-4.49×10^8 J m^{-3}) for $Al_3Sc(L1_2)$ and -8.78 meV atom^{-1} (-8.58×10^7 J m^{-3}) for $Al_3Li(L1_2)$. The values of $\Delta E_{elastic}$ are calculated from the coherency strains as previously explained. The maximum elastic strains along the [1 0 0] direction, 1.89 meV atom^{-1} (1.85×10^7 J m^{-3}) for $Al/Al_3Sc(L1_2)$ and 0.32 meV atom^{-1} (3.08×10^6 J m^{-3}) for $Al/Al_3Li(L1_2)$, are used to calculate R^* and $W_R^{homo}(R^*)$ (Eqs. (14) and (15)). These elastic internal strain energies are <4% of the total nucleation free energies of $Al_3Sc(L1_2)$ and $Al_3Li(L1_2)$. The quantity ΔF_V (Fig. 4) for $Al_3Sc(L1_2)$ and $Al_3Li(L1_2)$ is a function of temperature because of the entropic term, and both values of ΔF_V become positive for $T > 825$ K. The calculated values of ΔF_V in Fig. 4 are similar to the extrapolated results obtained by Hyland for $Al_3Sc(L1_2)$ [5].

The calculated values of R^* are 8.36 Å for Al_3Sc and 4.14 Å for Al_3Li, and the values of $W_R^{homo}(R^*)$ are 3.4 and 0.12 meV (5.43×10^{-22} and 1.87×10^{-23} J) for $Al_3Sc(L1_2)$ and $Al_3Li(L1_2)$, respectively. Fig. 4 demonstrates that formation of Al_3Li requires a smaller ΔF_V than that of Al_3Sc at a given temperature <350 K. Hyland et al. calculated smaller values of the Al_3Sc critical radius, 4.07 Å and a net reversible work, 3.0 meV (4.85×10^{-22} J), owing to their use of $\gamma = 94$ mJ m^{-2}; the latter value is from Monte Carlo simulations using embedded atom method potentials, and is lower than the first-principles $T = 0$ K calculated interfacial energy.

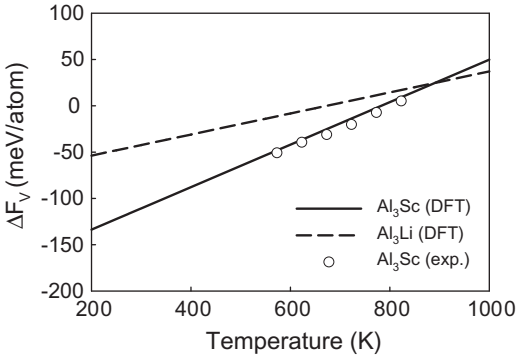

Fig. 4. The experimental and first-principles calculated nucleation free energy ΔF_V of Al_3Sc and Al_3Li as function of temperature (K). The calculated ΔF_V is in excellent agreement with Hyland's extrapolated results for $Al_3Sc(L1_2)$ [5].

To investigate the nucleation of core/shell morphologies, consider the case of heterogeneous nucleation, where an η-phase nucleates at the interface between the α and β phases. Three interfacial energies are important in this nucleation process: $\gamma_{\alpha/\beta}$, $\gamma_{\alpha/\eta}$ and $\gamma_{\beta/\eta}$. There are two wetting angles involved: θ_1 between α and η, and θ_2 between β and η. The angles θ_1 and θ_2 are involved in the balance of forces at the point of contact between the nucleus and the boundary, parallel and vertical to the contacting interface.

$$\gamma_{\alpha/\eta} \cdot \sin\theta_1 = \gamma_{\beta/\eta} \cdot \sin\theta_2 \tag{17}$$

$$\gamma_{\alpha/\eta} \cdot \cos\theta_1 + \gamma_{\beta/\eta} \cdot \cos\theta_2 = \gamma_{\alpha/\beta} \tag{18}$$

The angles θ_1 and θ_2 are then given by

$$\cos\theta_1 = \frac{\gamma_{\alpha/\beta}^2 + \gamma_{\alpha/\eta}^2 - \gamma_{\beta/\eta}^2}{2 \cdot \gamma_{\alpha/\beta} \cdot \gamma_{\beta/\eta}} \tag{19}$$

$$\cos\theta_2 = \frac{\gamma_{\alpha/\beta}^2 + \gamma_{\beta/\eta}^2 - \gamma_{\alpha/\eta}^2}{2 \cdot \gamma_{\alpha/\beta} \cdot \gamma_{\beta/\eta}} \tag{20}$$

There are two possible heterogeneous nucleation mechanisms: (1) $Al_3Li(L1_2)$ nucleates on $Al_3Sc(L1_2)$; or (2) $Al_3Sc(L1_2)$ nucleates on $Al_3Li(L1_2)$. In case 1, since $\gamma_{Al/Al_3Sc} \gg \gamma_{Al/Al_3Li}$ and $\gamma_{Al/Al_3Sc} > \gamma_{AlSc/Al_3Li}$, the wetting angles θ_1 and θ_2 for an $Al_3Li(L1_2)$ nucleus on an $Al_3Sc(L1_2)$ surface are 0°, implying that $Al_3Li(L1_2)$ completely wets an $Al_3Sc(L1_2)$ surface, and therefore nucleation is energetically preferred and barrierless. Alternatively, the value of θ_1 of an $Al_3Sc(L1_2)$ nucleus on an $Al_3Li(L1_2)$ surface is 180° and there is no wetting, which implies that $Al_3Sc(L1_2)$ cannot nucleate on an $Al_3Li(L1_2)$ surface. These results provide an explanation for the fact that $Al_3Li(L1_2)/Al_3Sc(L1_2)$ core/shell precipitates are not observed experimentally, but only $Al_3Sc(L1_2)/Al_3Li(L1_2)$ core/shell precipitates are observed [10].

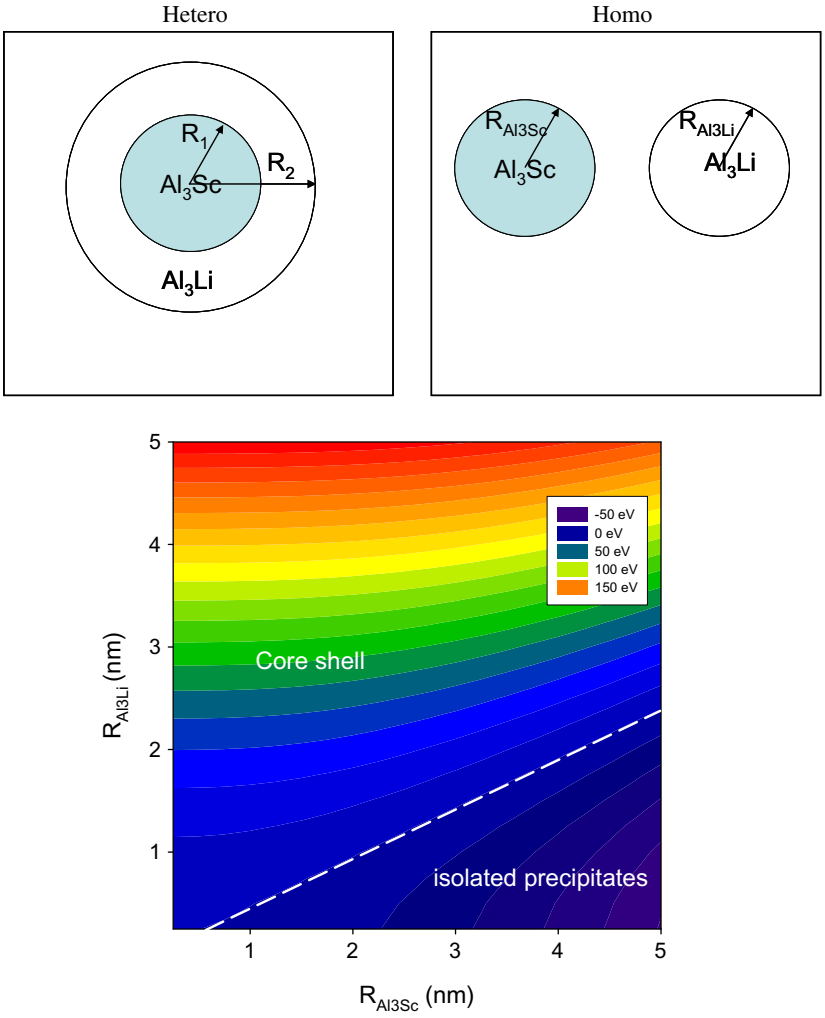

Fig. 5. The stability of core/shell precipitates of $Al_3Sc(L1_2)/Al_3Li(L1_2)$ in Al–Sc–Li alloys. Two morphologies are considered: (a) an $Al_3Sc(L1_2)/Al_3Li(L1_2)$ core/shell scenario (labeled "hetero"); (b) two separate $Al_3Li(L1_2)$ and $Al_3Sc(L1_2)$ precipitates (labeled "homo"). The energy $\Delta E = E_{homo} - E_{hetero}$ from DFT calculations shows that the heterogeneous core/shell scenario is more favorable than separate precipitates, in agreement with the experimental observations for an Al–Sc–Li alloy [10].

Please cite this article in press as: Mao Z et al. First-principles study of the nucleation and stability of ordered precipitates in ternary Al–Sc–Li alloys. Acta Mater (2011), doi:10.1016/j.actamat.2011.01.041

3.7. Energetic stability of precipitate morphologies: core/shell vs. isolated precipitate structures

The isolated nucleation of $Al_3Sc(L1_2)$ and metastable $Al_3Li(L1_2)$ precipitates was discussed above. $Al_3Li(L1_2)$ precipitates nucleate more readily than do $Al_3Sc(L1_2)$ precipitates in Al. The stability of core/shell precipitates is now discussed, based on the nucleation free energies and interfacial energies calculated. Core/shell precipitates are observed in dilute Al–Sc–Li alloys, thus it is important to compare the stabilities of core/shell precipitates with isolated precipitates. From the calculations, γ_{Al/Al_3Sc} is significantly greater than γ_{Al/Al_3Li} and γ_{Al_3Li/Al_3Sc}. $Al_3Li(L1_2)$ can completely wet an $Al_3Sc(L1_2)$ surface (wetting angle is 0°) if the concentration of Li is larger than that of Sc and the radius of Al_3Sc spherical precipitate is larger than its critical value 8.36 Å, but $Al_3Sc(L1_2)$ cannot wet an $Al_3Li(L1_2)$ surface (wetting angle is 180°). Thus, the Al_3Li(core)/Al_3Sc(shell) structure is energetically unfavorable. Therefore, only Al_3Sc (core)/Al_3Li(shell) and isolated $Al_3Sc(L1_2)$ and $Al_3Li(L1_2)$ precipitates are discussed. A model was constructed based on DFT energetics (Fig. 5) to compare the relative stabilities between the two possible precipitate morphologies in the Al–Sc–Li system. The two morphologies and their calculated energies are displayed in Fig. 5. First, two isolated $Al_3Li(L1_2)$ and $Al_3Sc(L1_2)$ precipitates are considered, labeled "homo", and then a core/shell structure, labeled "hetero". The energy difference between these two possibilities is as follows:

$$\Delta E = E_{homo} - E_{hetero} \tag{21}$$

$$E_{homo} = \frac{4}{3}\pi\left(R^3_{Al_3Li}\Delta F_{Al_3Li} + R^3_{Al_3Sc}\Delta F_{Al_3Sc}\right) + 4\pi\left(R^2_{Al_3Li}\gamma_{Al/Al_3Li} + R^2_{Al_3Sc}\gamma_{Al/Al_3Sc}\right) \tag{22}$$

$$E_{hetero} = \frac{4}{3}\pi\left[(R_2^3 - R_1^3)\Delta F_{Al_3Li} + R_1^3\Delta F_{Al_3Sc}\right] + 4\pi\left(R_1^2\gamma_{Al_3Li/Al_3Sc} + R_2^2\gamma_{Al/Al_3Li}\right) \tag{23}$$

The volume of the precipitates is a constant for both cases. It is found (Fig. 5) that the hetero core/shell case is energetically more favorable than isolated precipitates, provided that there is a sufficient Li concentration to cover the Al_3Sc core completely if the Li concentration is greater than the Sc concentration. A detailed study by APT of the chemical compositions of precipitates in the Al–Li–Sc system reveals two populations of precipitates [10]: larger Al_3Sc(core)/Al_3Li(shell) precipitates and isolated homogeneously distributed smaller $Al_3Li(L1_2)$ precipitates. The calculations are in agreement with these experimental observations. It is found that only individual $Al_3Sc(L1_2)$ precipitates are favorable when the Li concentration is less than the Sc concentration, that is, there is insufficient Li in the alloy to cover the Al_3Sc core.

4. Conclusions

The nucleation and stability of the precipitates in Al–Sc–Li alloys were systematically studied based on bulk thermodynamics (static total energies and vibrational free energies) and interfacial energies by first-principles calculations, leading to the following conclusions.

(1) The coherency strains of Al/Al_3Sc, Al/Al_3Li and Al_3Sc/Al_3Li structures are determined using a harmonic approximation. Owing to relatively small lattice parameter mismatches in these systems, all the calculated strain energies are small and contribute <4% to the total nucleation free energies of $Al_3Sc(L1_2)$ and $Al_3Li(L1_2)$.

(2) Lithium and scandium share the same sublattice sites in the $L1_2$-ordered structures, and the solubilities of Sc in $Al_3Li(L1_2)$ and of Li in $Al_3Sc(L1_2)$ are non-zero. This result is in excellent agreement with APT experiments [10,11], with the Li concentration varying from 12 to 21 at.% in the Al_3Sc core and Al_3Li shell after aging treatments.

(3) During precipitation, the energetically most favorable solute substitutional path involves diffusion of Li (or Sc) from the solid solution and substitution for Sc (or Li) in Al_3Sc (or Al_3Li). The related substitutional formation energies are −0.059 eV and −0.028 eV atom^{-1}, respectively. The displaced Sc (or Li) atom then leads to the precipitation of additional $L1_2$-ordered Al_3Sc (or Al_3Li) precipitates.

(4) The solubilities of Sc and Li in Al alloys are in good agreement with the experimental results and previous phonon vibrational calculations. The vibrational contributions to the free energies give a 14-fold increase in the calculated solubility of Sc in Al and a twofold increase in the calculated solubility of Li in Al when compared with the static-energy calculations.

(5) The interfacial energies of (1 0 0), (1 1 0) and (1 1 1) interfaces are obtained by both LDA and GGA methods. There is a small systematic shift of the interfacial energies, with GGA predicting consistently smaller interfacial energies than does LDA. This systematic shift is consistent with the well-known tendency of LDA to predict overbinding of a wide range of properties.

(6) The interfacial energy of Al/Al_3Sc (165 mJ m^{-2} for (1 0 0) plane from GGA) is significantly greater than that of Al/Al_3Li (12 mJ m^{-2} for (1 0 0) plane), and Al_3Sc/Al_3Li (83 mJ m^{-2} for (1 0 0) plane) interfaces, implying that the possible precipitate structures are: (1) isolated $Al_3Sc(L1_2)$ and $Al_3Li(L1_2)$ precipitates; and (2) a stable $Al_3Sc(L1_2)$/$Al_3Li(L1_2)$ core/shell structure, as observed experimentally.

(7) From CNT, the nucleation of $Al_3Li(L1_2)$ is much easier than $Al_3Sc(L1_2)$ at 350 °C. The calculated critical radius of $Al_3Li(L1_2)$ (4.14 Å) is smaller than that of

Please cite this article in press as: Mao Z et al. First-principles study of the nucleation and stability of ordered precipitates in ternary Al–Sc–Li alloys. Acta Mater (2011), doi:10.1016/j.actamat.2011.01.041

$Al_3Sc(L1_2)$ (8.36 Å). The critical net reversible work required is 3.4 and 0.12 meV (5.43×10^{-22} and 1.87×10^{-23} J) for $Al_3Sc(L1_2)$ and $Al_3Li(L1_2)$, respectively.

(8) If the Li concentration in the alloy is larger than the Sc concentration and the radius of $Al_3Sc(L1_2)$ spherical precipitate is greater than its critical value 8.36 Å, $Al_3Li(L1_2)$ will wet $Al_3Sc(L1_2)$, decreasing the interfacial energy of the system and leading to stable core/shell precipitates. Since the Sc solubility is small and the Li solubility is large, this core/shell structure is thermodynamically stable.

Acknowledgements

This work is supported by the Department of Energy, Office of Basic Energy Science, under Grant DE-FG02-98ER45721, monitored by Dr. John Vetrano. Wei Chen is supported by National Science Foundation under Contracts No. CBET-0730841 and No. CBET-0731020. The authors thank Prof. David C. Dunand for many helpful discussions, and Mr. Matthew E. Krug and Dr. Christopher Booth-Morrison for discussions of the APT results.

References

[1] Westwood A. Mater Sci Technol 1990;6:958.
[2] Drits ME, Toropova LS, Gushchina RL, Fedotov SG. J Sov Nonferrous Metals Res 1984;12:83.
[3] Marquis EA, Seidman DN. Acta Mater 2001;49:1909.
[4] Marquis EA, Seidman DN, Dunand DC. Acta Mater 2002;50:4021.
[5] Hyland Jr RW. Metall Trans A 1992;23A:1947.
[6] Harada Y, Dunand DC. Intermetallics 2009;17:17.
[7] Sanders TH. Aluminum–lithium alloys. Georgia: Stone Mountain; 1980.
[8] Beresina AL, Kolobnev NI, Chuistov KV, Kotko AV, Molebny OA. Mater Sci Forum 2002;396–402:977.
[9] Berezina AL, Volkov VA, Golub TV, Ivanov SV, Kashevskaya ON, Chuistov KV. Metallofizika (Kiev) 1991;13:54.
[10] Krug ME, Dunand DC, Seidman DN. Appl Phys Lett 2008;92.
[11] Krug ME, Werber A, Dunand DC, Seidman DN. Acta Mater 2010;58:134.
[12] Wolverton C, Ozolins V. Phys Rev B 2006;73.
[13] Ravi C, Wolverton C, Ozolins V. Europhys Lett 2006;73:719.
[14] Wolverton C. Philos Mag Lett 1999;79:683.
[15] Wolverton C, Ozolins V, Zunger A. J Phys Condens Matter 2000;12:2749.
[16] Wolverton C, Zunger A. Phys Rev B 1995;51:6876.
[17] Ozolins V, Sadigh B, Asta M. J Phys Condens Matter 2005;17:2197.
[18] Asta M, Ozolins V, Woodward C. JOM 2001;53:16.
[19] Asta M, Ozolins V. Phys Rev B 2001;6409.
[20] Asta MN, Ozolins V, Hoyt JJ, Van Schilfgaarde M. Phys Rev B 2001;6402.
[21] Sluiter M, Kawazoe Y. Phys Rev B: Condens Matter 1996;54:10381.
[22] Sluiter MHF, Watanabe Y, de Fontaine D, Kawazoe Y. Phys Rev B 1996;53:6137.
[23] Ozolins V, Asta M. Phys Rev Lett 2001;86:448.
[24] Perdew JP, Zunger A. Phys Rev B 1981;23:5048.
[25] Wu ZG, Cohen RE. Phys Rev B 2006;73.
[26] Kresse G. J Non-Cryst Solids 1996;205–207:833.
[27] Kresse G, Furthmueller J. Phys Rev B 1996;54:11169.
[28] Kresse G, Furthmuller J. Comput Mater Sci 1996;6:15.
[29] Kresse G, Hafner J. Phys Rev B 1993;47:558.
[30] Kresse G, Hafner J. Phys Rev B 1994;49:14251.
[31] Kresse G, Joubert D. Phys Rev B 1999;59:1758.
[32] Yin MT, Cohen ML. Phys Rev Lett 1980;45:1004.
[33] Ho KM, Fu CL, Harmon BN, Weber W, Hamann DR. Phys Rev Lett 1982;49:673.
[34] Lam PK, Cohen ML. Phys Rev B Condens Matter 1982;25:6139.
[35] Wolverton C, Ozolins V. Phys Rev B 2006;73:144104/1.
[36] Hyland RW, Asta R, Foiles SM, Rohrer CL. Acta Mater 1998;46:3667.
[37] Hyland RW, Stiffler RC. Scr Metall Mater 1991;25:473.
[38] Grobner J, Schmid-Fetzer R, Pisch A, Cacciamani G, Riani P, Parodi N, et al. Z Metall 1999;90:872.
[39] Cacciamani G, Riani P, Borzone G, Parodi N, Saccone A, Ferro R, et al. Intermetallics 1999;7:101.
[40] Guo XQ, Podloucky R, Freeman AJ. J Mater Res 1991;6:324.
[41] Woodward C, Asta M, Kresse G, Hafner J. Phys Rev B 2001;6309.
[42] Li Z, Tse JS. Phys Rev B Condens Matter Mater Phys 2000;61:14531.
[43] Laks DB, Ferreira LG, Froyen S, Zunger A. Phys Rev B 1992;46:12587.
[44] Ozolins V, Wolverton C, Zunger A. Phys Rev B 1998;57:6427.
[45] Ozolins V, Wolverton C, Zunger A. Phys Rev B 1998;57:4816.
[46] Vaithyanathan V, Wolverton C, Chen LQ. Acta Mater 2004;52:2973.
[47] Wang JW, Wolverton C, Muller S, Liu ZK, Chen LQ. Acta Mater 2005;53:2759.
[48] Varney CN, Hart GLW, Wolverton C. TMS Lett 2004;1.
[49] Wolverton C. Modell Simul Mater Sci Eng 2000;8:323.
[50] Muller S, Wang LW, Zunger A, Wolverton C. Phys Rev B 1999;60:16448.
[51] The authors emphasize that the $Al_3Li(L1_2)$ phase is metastable, so some combination of other non-fcc-based structures is lowest in energy for the Al–Li system; but constraining the discussion to the fcc-based structures, the $L1_2$ structure has the lowest energy of the compounds considered with Al_3Li stoichiometry.
[52] Hatch JE. Aluminum: properties and physical metallurgy. Metals Park, Ohio: American Society of Metals; 1998.
[53] Clouet E, Nastar M, Sigli C. Phys Rev B 2004;69.
[54] Clouet E, Nastar M. Phys Rev B 2007;75.
[55] Wright EH, Willey LA. Alcoa (Aluminum Co. Am) Res Lab, Technol Paper 1960:46.
[56] Drits ME, Kadaner ES, Dobatkina TV, Turkina NI. Izvestiya Akademii Nauk SSSR, Metall 1973;213.
[57] Fujikawa S, Sugaya M, Takei H, Hirano K. J Less-Common Metal 1979;63:87.
[58] Noble B, Thompson GE. Metal Sci J 1971;5:114.
[59] Williams DB, Edington JW. Metal Sci J 1975;9:529.
[60] Ceresara S, Cocco G, Fagherazzi G, Schiffini L. Philos Mag 1977;35:373.
[61] Ceresara S, Giarda A, Sanchez A. Philos Mag 1977;35:97.
[62] Cocco G, Fagherazzi G, Schiffini L. J Appl Crystallogr 1977;10:325.
[63] Nozato R, Nakai G. Trans Jpn Inst Metal 1977;18:679.
[64] Baumann SF, Williams DB. Aluminium–lithium alloys II. Warrendale (PA): AIME; 1984.
[65] Jensrud O, Ryum N. Mater Sci Eng 1984;64:229.
[66] Livet F, Bloch D. Scr Metall 1985;19:1147.
[67] Fujikawa S, Izeki Y, Hirano K. Scr Metall 1986;20:1275.
[68] Papazian JM, Sigli C, Sanchez JM. Scr Metall 1986;20:201.
[69] Valentine MG, Saunders J. Aluminium–lithium alloys V. Warrendale (PA): AIME; 1989.
[70] Shaiu BJ, Li HT, Lee HY, Chen HD. Metall Trans A – Phys Metall Mater Sci 1990;21:1133.
[71] Gomeiro P, Livet F, Lyon O. Aluminium–lithium alloys VI. Germany: Schaft; 1991.
[72] Pitcher PD, Stewart RJ, Gupta S. Scr Metall Mater 1992;26:511.
[73] Sato T, Kamio A. In: Proceedings of the 4th international conference on aluminium alloys; their physical and mechanical properties. Atlanta (GA): Georgia Institute of Technology; 1994.

[74] Delrio J, Plazaola F, Dediego N. Philos Mag 1994;69:591.
[75] Noble B, Bray SE. Acta Mater 1998;46:6163.
[76] Wolverton C, Zunger A. Phys Rev B 1999;59:12165.
[77] Sluiter M, Kawazoe Y. Phys Rev B 1996;54:10381.
[78] Asta M, Foiles SM, Quong AA. Phys Rev B 1998;57:11265.
[79] Marquis EA, Seidman DN, Asta M, Woodward C, Ozolins V. Phys Rev Lett 2003;91.
[80] Soisson F, Martin G. J Jpn Inst Metal 1999;12:757.
[81] Soisson F, Martin G. Phys Rev B 2000;62:203.
[82] Ratke L, Voorhees PW. Growth and coarsening: Ostwald ripening in materials processing. Springer; 2002.
[83] Fujikawa SI, Sugaya M, Takei H, Hirano K. J Less-Common Metal 1979;63:87.

Please cite this article in press as: Mao Z et al. First-principles study of the nucleation and stability of ordered precipitates in ternary Al–Sc–Li alloys. Acta Mater (2011), doi:10.1016/j.actamat.2011.01.041